A method to interpret induced seismicity clouds as a fracture network

Rike Köpke[1], Emmanuel Gaucher[1], Jörg Meixner[1] and Thomas Kohl[1]

[1] Karlsruhe Institute of Technology, Institute of Applied Geosciences, Geothermal Research, Karlsruhe, Germany

rike.beuster@gmail.com

Keywords: Discrete fracture network, Probability, Earthquake, Focal mechanism, EGS, Soultz.

ABSTRACT

We use the three-point method for determining preferred directions or surfaces within a cloud of earthquakes and we extend this method by introducing weighting factors depending on inter-event distance and on event magnitude. Besides, a new method of statistical analysis of seismic clouds is developed to provide pseudo spatial probability of an event-driven fracture network. This method also applies distance and magnitude weighting, but additionally allows using focal mechanisms. Both methods are first tested and validated on synthetic data, and then applied to the seismicity induced in 2000 during the hydraulic stimulation of the well GPK2 of the Soultz-sous-Forêts geothermal site. The results obtained at Soultz are comparable to results from previous works.

1. INTRODUCTION

Seismicity may be induced by human activity such as mining, geothermal energy production, oil and gas production, etc. These rock failures are evidences that highlight fracture or fault zones geomechanically perturbed in the subsurface. In enhanced geothermal fields or in oil and gas applications where forced fluid injection can take place, such seismogenic zones may be representative of preferential fluid circulation pathways (Sausse *et al.* 2010). Hence, to characterize and to attempt to image the reservoir, it is of importance to describe geometrically the seismicity once it has been correctly located. This constitutes the topic of the present work.

To highlight geometrical features in a seismic cloud, only the locations of the seismic events may be used. The three-point method (3PM) proposed by Fehler, House and Kaieda (1987) belongs to this family. However, this method lacks additional information associated with the earthquakes. For example, the focal mechanism of seismic events can indicate preferential slipping plane directions and also help to define discrete fracture networks (Cipolla *et al.;* Yu *et al.;* Eisner *et al.* 2010). Hence, we intend to use more earthquake attributes than only their location to constrain fracture network highlighted by seismic clouds. Our hypotheses are 1) the fracture network should go through the seismicity, 2) distant earthquakes are less likely to belong to similar fracture/fault unless the rupture size of earthquakes is in accordance with such distance, and 3) focal mechanism of earthquakes provide preferential orientation of fractures. According to the first two hypotheses, we extend the original 3PM. This method, however, can be strongly time and disk-space consuming, especially because shape correction of seismic clouds have to be done and retrieval of the spatial location of the fractures is a secondary result. Therefore, we developed a probabilistic approach based on all available attributes of each earthquake: location, magnitude, fault plane solution, which could also integrate other geometrical information linked to the description of the fault and fracture system of the considered zone.

We illustrate the procedure and show results obtained at Soultz-sous-Forêts (France) geothermal site on the seismicity induced during the GPK2 well stimulation performed in 2000.

2. METHODOLOGY

Two different techniques expected to highlight fractures in a seismic cloud were applied and are described in the following.

2.1 The three-point method

The 3PM combines each event of a given dataset with two others to gain every possible combination of three events. Therewith, N triangles are generated, where N can be calculated from the number of events P. For each triangle, the normal vector is calculated to determine its orientation. The most represented orientations within the available dataset are supposed to be associated with preferential orientations of faults and fractures in the seismic cloud. To determine these orientations, the density of all vectors is calculated after equal-area discretization of the hemisphere with several bins, as presented in Fryer (1975). Each normal vector falling within a given bin is assigned to it. Then, the bins associated with the highest number of normal vectors show the preferential orientations. To account for the shape effect of the seismic cloud, the normalization method of Fehler *et al.* (1987) is applied. It consists in randomly generating several sets of earthquake hypocentres in the volume defined by

the original cloud and to scale the initial raw result by the random draw results (more details can be found in Fehler *et al.* 1987).

We extended the 3PM presented above by a relative weighting on distances and magnitudes. First, the concept is to assign a different weight to the triangle normal as a function of the distance between events constituting the triangle, the weight decreasing with increasing inter-event distance. Physically, this means that they are more chances for two nearby earthquakes to be connected than two far earthquakes. A Gaussian-like weighting function was used:

$$p_d = \exp(-d^2/2\sigma^2) \quad [1]$$

where d is the length of the largest triangle side and σ is the distance scaling free parameter. Its influence is discussed later.

Second, instead of distances, one can also consider magnitudes. According to Madariaga (1976), there is a connection between corner frequency and the size of the plane of rupture. One can also deduce a correlation between corner frequency and magnitude which is described by Charléty *et al.* (2007) for the site of Soultz. Thus, one can assign a minimal radius r of the plane of rupture for every earthquake of magnitude M. Accordingly, if all three events of a triangle of the 3PM lie within one of the radius of the other events, one can with certainty say that those events belong to the same plane of rupture and the triangle normal as a weight of 1. If this is not the case a Gaussian-like distance weighting function was used:

$$p_M = \exp\left(-(d^2 - r(M)^2)/2\left(\frac{r(M)}{Div}\right)^2\right) \quad [2]$$

where d is the distance between two points and r is the radius of one of those points which was calculated above. The values of d and r(M) are taken so that the value of W is minimal for all point combinations of the triangle. Div is a scaling free parameter.

2.2 Pseudo spatial probability density function

Contrarily to the 3PM, which focuses on preferred fault and fracture directions, we propose another approach that keeps the spatial information associated with the location of the earthquake hypocentres and processes the earthquakes independently, one after each other. This method first discretizes the 3D volume containing the seismicity of interest by cubic cells of 50-m edge. The cell size is of the order of the size of the earthquake location uncertainties. From a given earthquake hypocentre, pseudo-probability density functions (PPDF) of fracture or fault going through the associated cell are computed everywhere in the 3D mesh taking into account distance to that cell, magnitude of the earthquake and, if available, earthquake focal mechanism.

For distances, a PPDF similar to equation [1] is used, where d now represents the distance between the current earthquake cell and any other cell. Each earthquake is processed and the obtained PPDFs are summed. Thus, high final pseudo-probability values are obtained for cells close to a high earthquake density. For the magnitude weighting, an equation similar to equation [2] is applied, where r stands for the derived minimal radius of the plane of rupture for the considered earthquake. Hence, each earthquake would surely connect all neighboring cells contained within its source radius and then connection probability would decrease with increasing distance. Again, the summation of the PPDFs associated with each earthquake provides a final pseudo-probability. When the focal mechanism of an earthquake is available, it is possible to include directional information of the preferred rupture plane going through an earthquake. To do so, we apply a Gaussian-like weighting function depending on the angle α between the fault plane and the direction between the current earthquake cell and any other cell:

$$p_f = \exp\left(-\alpha^2/2{\sigma_f}^2\right) \quad [3]$$

where σ_f is a free parameter that affects the shape of the probability distribution. Therefore high cell values occur when those cells lie on the extended fault planes of many points.

For a given earthquake, the distance-/magnitude-PPDFs are direction independent and the focal mechanism-PPDF is distance independent. To make the most of both types of information, which are supposed to be independent, the PPDFs can be combined by multiplying both PPDF types to obtain distance and direction dependencies. Only once this multiplication is done, summation of the results for all earthquakes could be done to obtain the final pseudo-probability.

3. APPLICATION

3.1. Synthetic case

The described methods were first applied on synthetic datasets to confirm their functionality, to test the influence of the weighting parameters and to evaluate the results to real datasets.

The parameter σ (equation [1]) is varied from 0.05 to 0.1, 0.15 and 0.2; the parameter Div (equation [2]) from 0.5 to 1, 2 and 3. For this purpose, 10 artificial datasets were designed which can be divided into 3 groups (see **Table 1**). In each case a spherical cloud of 500 randomly distributed events with a radius of 1 is generated. Group 1 contains four datasets with one plane of 1 length and 0.5 width placed in the middle of the cloud. This plane is tilted 45° to the south and therefore has the orientation 45/180 (dip/dip direction in °). For dataset 1a this plane contains 100 of the 500 events, for dataset 1b 50 events, for dataset 1c 20 events and for dataset 1d 10 events. Group 2 and Group 3 contain two fracture planes positioned close to the border of the cloud. In the former case the planes are orthogonal, in the latter, they are parallel.

Table 1 gives all other characteristics of the groups and sets of events.

Table 1: Characteristics of the 10 synthetic fracture sets.

Plane description (plane #; size; orientation)	Set	# of events per plane
Group 1: 1 plane	1a	100/500
Plane #1; 1l × 0.5w; 45/180	1b	50/500
	1c	20/500
	1d	10/500
Group 2: 2 orthogonal planes	2a	50×2/500
Plane #1; 0.5l × 0.3w; 45/180	2b	20×2/500
Plane #2; 0.5l × 0.3w; 45/270	2c	10×2/500
Group 3: 2 parallel planes	3a	50×2/500
Plane #1; 0.5l × 0.3w; 45/180	3b	20×2/500
Plane #2; 0.5l × 0.3w; 45/180	3c	10×2/500

The application of the extended 3PM on the artificial datasets shows that the consideration of the distance between the events greatly improves the classical 3PM (Figure 1). The orientation of the planes was correctly identified for all chosen values of σ (0.05, 0.1, 0.15, 0.2) for all datasets except 1d and 2c, whereas with the classical 3PM the orientations could be clearly identified only for the datasets 1a and 1b. The original 3PM is not suitable for identifying multiple planes, especially when they are separated by distances larger than their size. As a matter of fact, the relatively high density of events on the planes does not compensate the large number of triangles between the two planes which leads to wrong plane direction identification.

When the event magnitudes, which are randomly distributed in the cloud, are considered, only a value of Div = 0.5 leads to acceptable results, i.e. the orientations of the planes are determined correctly for all datasets except dataset 1d. For all other Div values (1, 2, 3), which correspond to steeper decline of the PPDF with the distance, orientations of planes different from the expected ones were obtained as preferential orientations or in addition to the expected orientations. This effect is due to the fact that high pseudo-probabilities exist only for three-points located inside the range of the magnitude-depending radius of at least one other event; and the density of points on the predefined plane(s) is not sufficient to compensate this behaviour in most cases. Nevertheless it has to be noticed that for the artificial dataset the magnitudes are randomly distributed in the cloud whereas in a real dataset this is probably not the case. If the magnitudes of events located on dominant geological structures are higher than the magnitudes of the surrounding events it might be possible to connect them to each other and to identify the orientation of these structures.

To conclude on the extended 3PM, it seems that implementation of the distance weighting provides better identification of existing fracture orientations than the magnitude weighting (at least for the synthetic dataset).

The application of the distance PPDF shows good results for all datasets “a” and suitable results for all datasets “b” (Figure 1). The planes can be recognized for all values of σ, but the higher the value is, the larger is the area of high pseudo-probabilities around the planes and the less precise the position, the size and the orientation of the planes can be determined. On the other hand, if the density of the events on a large plane is rather low, like in dataset 1b, small values for σ can lead to the effect that the large plane seems to be split up in two or more smaller planes. This effect is stronger when the magnitude is considered. For Div = 0.5 and 1, the planes of the datasets 1a, 2a and 3a are well identified (Figure 1) whereas for Div = 2 and 3, only small areas on the planes were highlighted like a cluster of scattered maxima of high pseudo probabilities. For the datasets “b” the planes can also be identified for Div = 0.5 and 1 but much less clear as for all “a” datasets. To test the influence of the focal mechanism, each event on a plane is assigned the orientation of the rupture plane, all other events are assigned random orientations. For σ_f the value 5 is chosen. The combined distance-focal mechanism PPDF shows very good results for all values of σ for the datasets “a” and “b” and also for the dataset 1c the plane can be identified. The areas of high pseudo probabilities around the planes, which were quite large for large values of σ, are now much slimmer (Figure 1). This allows a better determination of the size and orientations of the planes that are now very close to the expected ones. The combined magnitude-focal mechanism PPDF also shows good results, especially for Div = 0.5. For Div = 1, 2 and 3 the directional constraint brought by the focal mechanism has only a minor influence because there are no widespread areas of pseudo-probabilities around the planes.

Every event on a synthetic plane has exactly the orientation of the corresponding plane which is not likely for real data. Accordingly, geological structure identification on real data may be less clear.

3.2. Soultz-sous-Forêts

3.2.1. Earthquake reference catalogue

We apply the proposed methodology to the deep geothermal reservoir of Soultz-sous-Forêts (France) which is located in the Upper Rhine Graben. For the development of this enhanced geothermal system, four wells have been drilled and stimulated by massive water injection to create the underground heat exchangers prior to production (Genter *et al.* 2010). Here, we focus on the seismicity which was induced in 2000 during the water stimulation of the well GPK2. The objective of the water injection of 23,400 m³ over 6 days was to increase the permeability of the granite, at 5 km depth, thus the well productivity. This operation was seismically monitored and the induced seismicity recorded by the surface and downhole monitoring networks was jointly processed by Cuenot, Dorbath and Dorbath (2008).

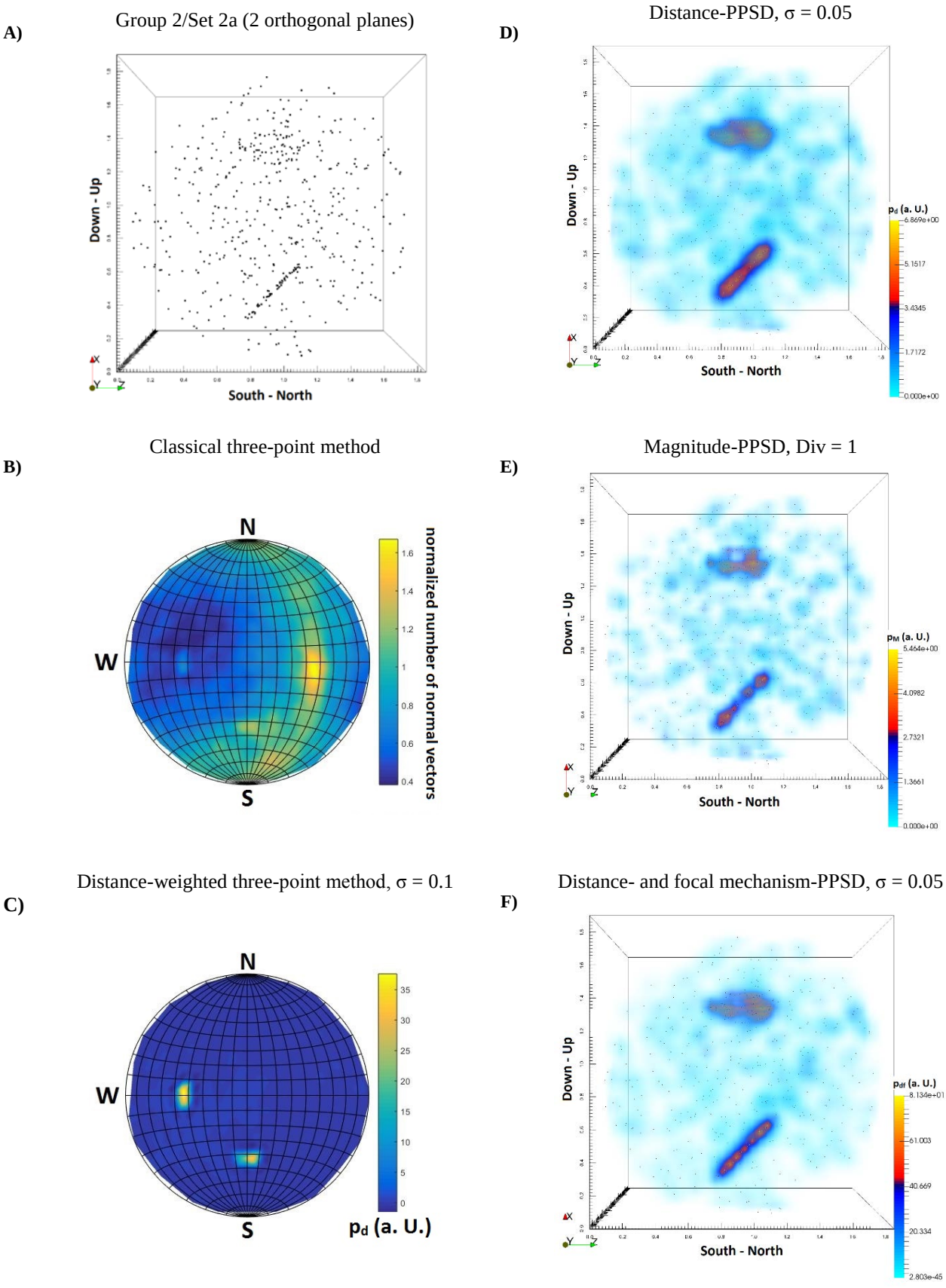

Figure 1: Results of the synthetic test for Group 2/Set 2a: 2 orthogonal planes with 50 among 500 events per plane; Plane #1: 0.5l × 0.3w with 45/180 orientation and Plane #2: 0.5l × 0.3w with 45/270 orientation. A) 3D-view of the synthetic cloud; results of B): 3PM, C) distance-weighted 3PM with σ = 0.1, D) distance-PPSD with σ = 0.05, E) magnitude-PPSD with Div = 1, and F) distance- and focal mechanism-PPSD with σ = 0.05.

In total, 7215 seismic events with a maximum moment magnitude M_W of 2.5 were located and for 715 of them, all with $M_W > 1$, the focal mechanisms were computed (Dorbath *et al.* 2009; Schoenball *et al.* 2012). The hypocentre location of the 7215 events was recomputed by Calò *et al.* (2011) in the course of a 4D tomographic inversion. These 7215 locations and magnitudes as well as the focal mechanisms of the 715 largest events computed by Cuenot, Dorbath and Dorbath (2008) constitute the reference databases on which we intend to highlight a fracture network.

3.2.2. Results and discussion

First, the 3PM without any consideration of distance and magnitude is applied, then distance weighting is introduced with σ = 0.05, 0.1, 0.15 and 0.2, and at last the magnitude weighting is introduced with Div = 0.5, 1, 2 and 3.

For the big dataset, the results are quite consistent for the classical approach and that with distance weighting for all values of σ (Figure 2). Two sets of steeply dipping orientations are identified, one to WSW and one to ENE, with maxima for orientations 82/250 and 88/067 respectively. The WSW-set is slightly dominating. The application of the magnitude weighting for Div = 0.5 provides results consistent with the previous ones. There are also two sets of preferred orientations with the maxima 81/243 and 82/065. For Div = 1, the previously identified sets of preferential orientations are replaced by clusters of scattered medium-high PPDF in W to SW and NE directions. For Div = 2 and 3 no preferential orientations is identified.

For the small dataset, the results are not as consistent as for the big one. The 3PM without consideration of distance or magnitude highlights three southern orientations around 38/141, 64/212 and 40/196. These are not identified as preferential orientations for the big dataset and also not for the small dataset under consideration of the distance for σ = 0.05, 0.1 and 0.15. Merely for σ = 0.2 a 61/190 southward dipping plane is highlighted. For σ = 0.05 relatively high pseudo-probabilities are scattered over the whole plot but especially in the W to SW and the NE sectors. For σ = 0.1, 0.15 and 0.2 the two sets of steep dipping orientations to WSW and NE seen for the big dataset are also recognisable despite less distinct and despite the orientation of the maxima are less consistent for the different parameters (Figure 2). Especially for σ = 0.2, additional high pseudo-probabilities for southern orientations are highlighted. The magnitude weighting leads to more deviating results. Only for Div = 0.5, the two dominating sets with WSW and NE orientations are recognisable (at 69/261 and 79/055). For Div = 1, 2 and 3, no preferential orientation is identified.

The (extended) 3PM results show that two steeply dipping orientations are dominating within the GPK2 seismic cloud, one dipping to WSW, around 82/250, the other dipping to NE, around 88/067. For the small dataset also southward orientations may be observed as well as other orientations not connected with the dominating ones.

In a second step, the PPDF is applied. On the big dataset, the distance-PPDF gives nearly to the whole cloud of events high pseudo-probability for σ larger than 0.1. Only for σ = 0.05, preferred connected regions in the cloud are distinguishable (Figure 2). The largest pseudo-probability values form a roughly ellipsoid-like area in the lower-northern part of the cloud with an orientation of 83/249, which is consistent with the results from the 3PM. The magnitude-PPDF with Div = 0.5 provides results similar to the distance-PPDF ones with σ = 0.05. With increasing Div values, the volume splits up in smaller and smaller features with higher and higher pseudo-probabilities (Figure 2).

The computation of the PPDFs for the small dataset leads to results similar to those obtained for the big dataset. An area of high pseudo-probabilities in the lower-northern part of the cloud with an asymmetric ellipsoid shape of main orientation 83/248 can be observed and is consistent with the results from the 3PM. Beside this dominating feature, two areas in the southern part of the cloud one above the other are visible.

For the small dataset, the focal mechanisms are available and the focal mechanism-PPDF can be computed and combined to the distance- and magnitude-PPDFs. We select the parameters $\sigma_f = 5$, σ = 0.1 (Figure 2) and Div = 0.5. The joint PPDFs show slightly different results than before. The combination of distance and focal mechanism gives high pseudo-probabilities in the lower-northern part of the cloud, which is stretched farther to the south and is connected with the lowest of the secondary high pseudo-probabilities regions. The orientation of this feature is 85/064 and therefore changed from westward to eastward dipping. This is consistent with the results from the 3PM which also show a steeply NE-ward dipping set of orientations. For the combination of magnitude and focal mechanism, the shape and the orientation of the area with high pseudo-probabilities is also slightly changed compared with that obtained from magnitude-PPSD only. The orientation is now 87/247.

In summary, all applied methodologies (3PM, extended 3PM or to PPDFs) highlight a dominating feature in the lower-northern part of the GPK2 seismic cloud with WSW-ward dipping orientation around 83/249. The size and detailed shape of this feature however vary strongly between the different parameters chosen. For low distance- and magnitude-weighting there seems to be one large structure in the dimension of several hundred meters whereas for high values the feature is divided into several smaller structures. The major feature is consistent with the major fault GPK2-2000a identified by Sausse *et al.* (2010) and oriented 86/244. The smaller structures may also be consistent with the GPK2-2000b fault suspected by Sausse *et al.* (2010).

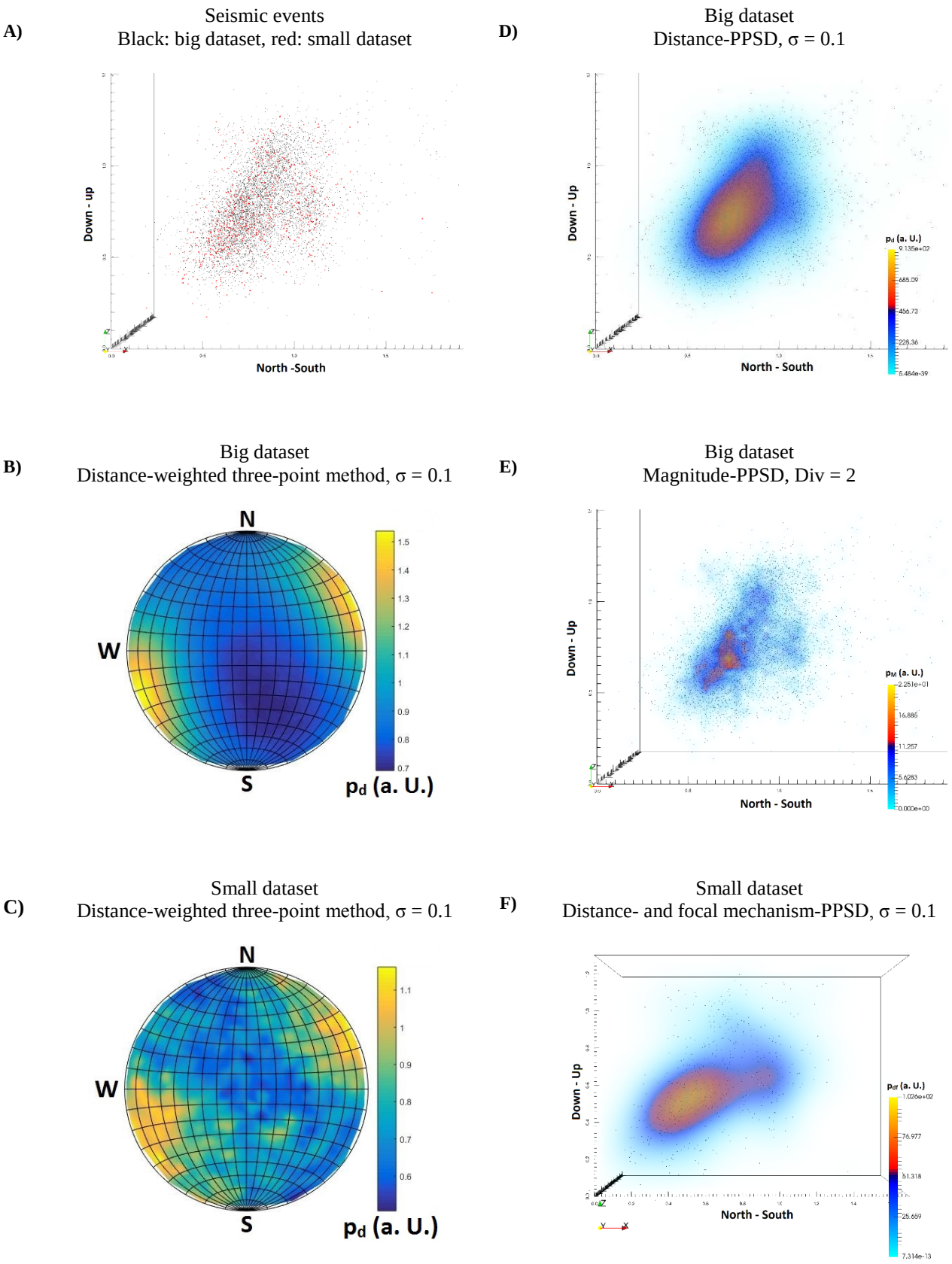

Figure 2: Results on the Soultz-GPK2-2000 seismic cloud. A) 3D-view of the induced seismicity; results of B) big dataset and distance-weighted 3PM with σ = 0.1, C) small dataset and distance-weighted 3PM with σ = 0.1, D) big dataset and distance-PPSD with σ = 0.1, E) big dataset and magnitude-PPSD with Div = 2, and F) small dataset and distance- and focal mechanism-PPSD with σ = 0.1.

3. CONCLUSION

We described and proposed two main methodologies to identify planar features in seismic clouds. The three-point method, which is dedicated to the identification of normals to planes, was extended to take into account distance separating earthquakes and earthquake magnitude. The synthetic test showed that this is a valuable implementation which can improve the results. A pseudo-probability density function associated with every earthquake and depending on the distance to this earthquake, its magnitude and its focal mechanism was presented. Contrarily to the three-point method, this approach provides spatial results at a smaller cost. The synthetic test also proved its effectiveness and highlighted the consistency of the results between both approaches. The application of both methodologies to the seismicity induced at Soultz-sous-Forêts, during the water stimulation of the well GPK2 in 2000, also provided consistent results. The main feature with a dip of 83° and dip direction 249° which is identified by the extended three-point method is also observed from the pseudo-probability maps. The spatial details given by the pseudo-probability density function are also consistent with results obtained by previous studies, which discuss a major fault zone in the deeper-northern part of the cloud.

REFERENCES

Calò M., Dorbath C., Cornet F.H. and Cuenot N. 2011. Large-scale aseismic motion identified through 4-D P-wave tomography. *Geophysical Journal International* **186** (3), 1295–1314.

Charléty J., Cuenot N., Dorbath L., Dorbath C., Haessler H. and Frogneux M. 2007. Large earthquakes during hydraulic stimulations at the geothermal site of Soultz-sous-Forêts. *International Journal of Rock Mechanics and Mining Sciences* **44** (8), 1091–1105.

Cipolla C.L., Williams M.J., Weng X., MacK M.G. and Maxwell S.C. Hydraulic Fracture Monitoring to Reservoir Simulation: Maximizing Value, SPE. Society of Petroleum Engineers. ISBN 978-1-55563-300-4.

Cuenot N., Dorbath C. and Dorbath L. 2008. Analysis of the microseismicity induced by fluid injections at the EGS site of Soultz-sous-Forêts (Alsace, France): Implications for the characterization of the geothermal reservoir properties. *Pure and Applied Geophysics* **165** (5), 797–828.

Dorbath L., Cuenot N., Genter A. and Frogneux M. 2009. Seismic response of the fractured and faulted granite of Soultz-sous-Forêts (France) to 5 km deep massive water injections. *Geophysical Journal International* **177** (2), 653–675.

Eisner L., Williams-Stroud S., Hill A., Duncan P. and Thornton M. 2010. Beyond the dots in the box: Microseismicity-constrained fracture models for reservoir simulation. *The Leading Edge* **29** (3), 326–333.

Fehler M., House L. and Kaieda H. 1987. Determinating planes along which earthquakes occur: method and application to earthquakes accompanying hydraulic fracturing. *Journal of Geophysical Research* **92**, 9407–9414.

Fryer R.J. 1975. On the subdivision of a spherical surface into elements of equal area. *Geophysical Journal of the Royal Astronomical Society* **42**, 883–891.

Genter A., Evans K., Cuenot N., Fritsch D. and Sanjuan B. 2010. Contribution of the exploration of deep crystalline fractured reservoir of Soultz to the knowledge of enhanced geothermal systems (EGS). *Comptes Rendus Geoscience* **342** (7-8), 502–516.

Madariaga R. 1976. Dynamics of an expanding circular fault. *Bulletin of the Seismological Society of America* **66** (3), 639–666.

Sausse J., Dezayes C., Dorbath L., Genter A. and Place J. 2010. 3D model of fracture zones at Soultz-sous-Forêts based on geological data, image logs, induced microseismicity and vertical seismic profiles. *Comptes Rendus Geoscience* **342** (7-8), 531–545.

Schoenball M., Baujard C., Kohl T. and Dorbath L. 2012. The role of triggering by static stress transfer during geothermal reservoir stimulation. *Journal of Geophysical Research* **117** (B9), B09307.

Yu X., Rutledge J., Leaney S. and Maxwell S. Discrete Fracture Network Generation from Microseismic Data using Moment-Tensor Constrained Hough Transforms, SPE. Society of Petroleum Engineers. ISBN 978-1-61399-310-1.

Acknowledgements

We thank M. Calò as well as L. Dorbath and C. Dorbath for providing the Soultz seismic data catalogues used in this study.